

On the physics of transient ejection from bubble bursting

Alfonso M. Gañán-Calvo^{1,2†}, and José M. López-Herrera¹

¹Dept. Ingeniería Aeroespacial y Mecánica de Fluidos, Universidad de Sevilla.
Camino de los Descubrimientos s/n 41092, Spain.

²Laboratory of Engineering for Energy and Environmental Sustainability,
Universidad de Sevilla, E-41092 Sevilla, Spain

(Received xx; revised xx; accepted xx)

The transient ejection due to a bubble bursting at the interface of a liquid with a gas environment is here described using a dynamical scaling analysis along the process. We show here that the ejection of a liquid microjet requires the backfire of a vortex ring inside the liquid to preserve physical symmetry, which involves a non-trivial scaling. Not only the size and speed of ejected droplets is predicted for the whole range of the Ohnesorge and Bond numbers where droplet ejection occurs, but also the evolution of the flow variables, the appearance of a singularity for a critical Ohnesorge number, and its maximum value for drop ejection are explained. Our model generalizes or displaces other recently proposed ones.

1. Introduction

Everyday experience teaches that radially convergent flows close to a liquid surface produce vigorous transient liquid ejections in the form of a jet perpendicular to the surface, as those seen after bubble bursting (Kientzler *et al.* 1954), droplet impact on a liquid pool (Yarin 2006), or cavity collapse (Ismail *et al.* 2018). The mechanical energy of the flow comes from the free surface energy of the initial cavity. Among these processes, bubble bursting can be considered the parametrically simplest (just two non-dimensional parameters, v.g. the Ohnesorge (oh) and Bond (Bo) numbers determine the physics and the outcome) and most ubiquitous one, and has received a special attention in the scientific literature due to its impact at global planetary scales (bubble bursting at the sea surface, e.g. Kientzler *et al.* (1954); Blanchard & Woodcock (1957); Veron (2015); Sampath *et al.* (2019); disease and pandemic transmission, e.g. Bourouiba (2021)) and in more indulging applications (e.g. Ghabache *et al.* (2016); Séon & Liger-Belair (2017)).

Current works state that the subject is already deeply understood (Berny *et al.* 2020; Sanjay *et al.* 2021). Yet, despite optimistic statements, even in the simplest case where the liquid properties are constant and the gas-to-liquid density and viscosity ratios are very small, unsettling but crucial questions remain open. Within an ample range of Oh and Bo, bubble bursting exhibits a strong focusing effect due to the nearly cylindrical collapse of a main wave at the bottom of the parent bubble. In these cases, a tiny bubble gets trapped and an extremely thin and rapid spout emerges. That initial spout grows into a much taller, thicker and slower transient jet that may eventually expel droplets. Their eventual size and speed is determined by Oh and Bo. However, for a critical Oh, the initial spout keeps its large speed and extremely thin radius until it ejects a nearly invisible droplet, such that the spout momentum (proportional to its velocity times

† Email address for correspondence: amgc@us.es

its volume) vanishes. Strikingly, a nearly symmetric behavior is observed around that critical Oh (Séon & Liger-Belair (2017), fig. 16). The possible existence of a mathematical singularity that may explain this phenomenon is dismissed by many. In reality, around that special parametrical region, compressibility and possibly nonlinear surface effects set in and the experiments exhibit a strong dispersion that may be reduced relying to local viscous effects and interaction with the gas environment (Brasz *et al.* 2018; Dasouqi *et al.* 2021). Yet, the question remains unanswered: Since a singularity would imply arbitrarily large speeds and vanishing sizes, could it have evaded accurate, systematic observation? Appealing to the facts, the global streamlines of the flow resemble a dipole with its axis perpendicular to the interface (figure 1). In general, the energy excess of the convergent flow leads to *both* a fast transient *capillary jet* and a *vortex ring* in opposite directions but equivalent effective momenta by virtue of Newton’s third law of motion. Their radically different kinematics, due to a large density disparity across the interface, is not an obstacle to their profound symmetry, as we will show here. This symmetry and its scalings are the keys to determine the eventual ejected droplet size and speed, and the appearance of singularities. These crucial observations cannot be accommodated by recent proposals (Gordillo & Rodriguez-Rodriguez 2019).

In this work, we present: (i) A universal non-trivial scaling of the evolution of the flow kinematic variables (characteristic lengths and velocity) and of the eventual ejected droplet size and speed, for the complete range of Oh for which ejection occurs (which generalizes Gañán-Calvo (2017)); (ii) The existence of a critical Oh (parametrical singularity) explaining the physical observations; (iii) A theoretical maximum value of the Oh to have droplet ejection. Our theoretical results are carefully validated against existing data from prior works (e.g. those collected in Gañán-Calvo (2017); Brasz *et al.* (2018); Gañán-Calvo (2018); Deike *et al.* (2018); Berny *et al.* (2020)) and novel numerical simulations.

2. Formulation and dynamical scaling analysis

Consider a gas bubble of initial radius R_o tangent to the free surface of a liquid with density, surface tension and viscosity ρ , σ and μ , respectively, in static equilibrium under a relatively small action of gravity acceleration g normal to the free surface far from the bubble. The flow properties are considered constant. At a certain instant, the thin film at the point of tangency breaks and the process of bubble bursting starts. The problem is thus determined by the Ohnesorge ($Oh = \frac{\mu}{(\rho\sigma R_o)^{1/2}}$) and Bond ($Bo = \frac{\rho g R_o^2}{\sigma}$) numbers alone. The liquid rim that is initially formed pilots two main capillary wave fronts, one that advances along the bubble surface towards its bottom, and the other propagating away from the cavity. In some parametrical regions of the domain $\{Bo, Oh\}$ of interest, those main waves may form wavelets at their front as those produced by the capillary rollers and bores described by Longuet-Higgins (1992). These wavelets may arrive first to the bottom, but do not produce any significant effect compared to the collapsing main wave (Gañán-Calvo 2018) in the parametrical domain here considered. When the main wave front approaches the bottom, it becomes steep. If the wave front leads to a nearly cylindrical collapsing neck in a certain region, a tiny bubble gets trapped below the surface once the ejection process commences. This process of radial collapse and bubble trapping is locally described by the theory of Eggers *et al.* (2007), Fontelos *et al.* (2011), and Eggers & Fontelos (2015) when a strong asymmetry in the axial direction occurs. This asymmetry is precisely the responsible of the initial extremely rapid and thin ejection in the opposite direction from the trapped bubble.

Figure 1 shows three illustrating instants of the flow development around the critical

instant t_0 at which the axial speed of the liquid surface on the axis reaches its maximum (immediately after the tiny gas neck collapses). When $t < t_0$, the flow is predominantly radial with a characteristic speed W at the interface. After collapse ($t > t_0$), while the main flow keeps running radially with speed W , the axial asymmetry of the flow and the kinetic energy excess of the liquid is axially diverted in the two opposite directions, with radically different results: (i) towards the open gas volume, producing the liquid spout with speed V and characteristic radial length R ; and (ii) towards the liquid bulk, as a backward reaction vortex ring (fig. 1b, in colors) with characteristic length L , around the trapped microbubble. Eventually, the advancing front of the resulting capillary jet expels a droplet or droplet train scaling as R .

Obviously, all scales $\{W, V, R, L\}$ are time-dependent. Prior works (e.g. Zeff *et al.* (2000); Lai *et al.* (2018)) have focused on time self-similarity of flow variables, arriving to fundamental universalities characterizing their evolution. Assuming that those time self similarities exist, our focus is here to obtain closed relationships among those scales and to predict the size and speed of ejections reflected by the eventual values of R and V at the end of the process. This approach, though, demands the identification of the key symmetries appearing in the problem that may lead to an effective problem closure (Gañán-Calvo *et al.* 2013). To this end, in Gañán-Calvo (2017, 2018) a set of relations among the radial and axial characteristic lengths and velocities is formulated on the basis that inertia, surface tension and viscous forces should be comparable very close to the instant of collapse of the free surface. While the previously proposed simple relations were fundamentally consistent, a rigorous derivation is here offered under the light of detailed numerical simulations. We will show that the formulated scale relationships not only hold at specific instants of their development, but throughout the entire process, for all Oh values of interest.

2.1. An integral relations-based dimensional analysis

The momentum equation of the liquid can be written as:

$$\rho \mathbf{v}_t + \nabla (p - P_a + \rho \mathbf{v}^2/2 + \rho g z) = \mathbf{v} \wedge \nabla \wedge \mathbf{v} + \mu \nabla^2 \mathbf{v}, \quad (2.1)$$

where \mathbf{v} is the velocity vector, subindex t denotes partial derivative with time, p is the liquid pressure, z the axial coordinate, \mathbf{n} the unit normal on the liquid surface, and P_a the static gas pressure. Although numerical simulations using *Basilisk* to obtain figures 1 take into account the gas motion, the gas density and viscosity are much smaller than those of the liquid. Thus, the dynamical effects are assumed negligible for the purpose of the following analysis.

Equation (2.1) can be multiplied by the unit vector \mathbf{l} tangent to any instantaneous streamline, in particular the streamline flowing through a point A where it meets the free surface to a point B at the vicinity of the point of collapse (see figure 1(a)). Integrating with respect to the streamline coordinate s from A to B yields:

$$\rho \int_A^B \mathbf{l} \cdot \mathbf{v}_t ds + \sigma \nabla \cdot \mathbf{n}|_B + \rho \mathbf{v}^2/2|_B + \rho g \Delta z|_A^B = \mu \int_A^B \mathbf{l} \cdot \nabla^2 \mathbf{v} ds, \quad (2.2)$$

since the velocity is negligible at A, and pressure is P_a . Δz is the depth of point B respect to A. As a general consideration, the liquid velocities are very small everywhere compared to the velocity at distances L to the collapsing region, which may exhibit a self-similar flow structure (Zeff *et al.* 2000; Duchemin *et al.* 2002; Lai *et al.* 2018). The length scale L also characterizes the inverse of the mean local curvature of the liquid surface around the region of collapse, for any given time t . Incidentally, L is also the scaling of the boundary layer due to the main wave (Gañán-Calvo 2018), supporting the

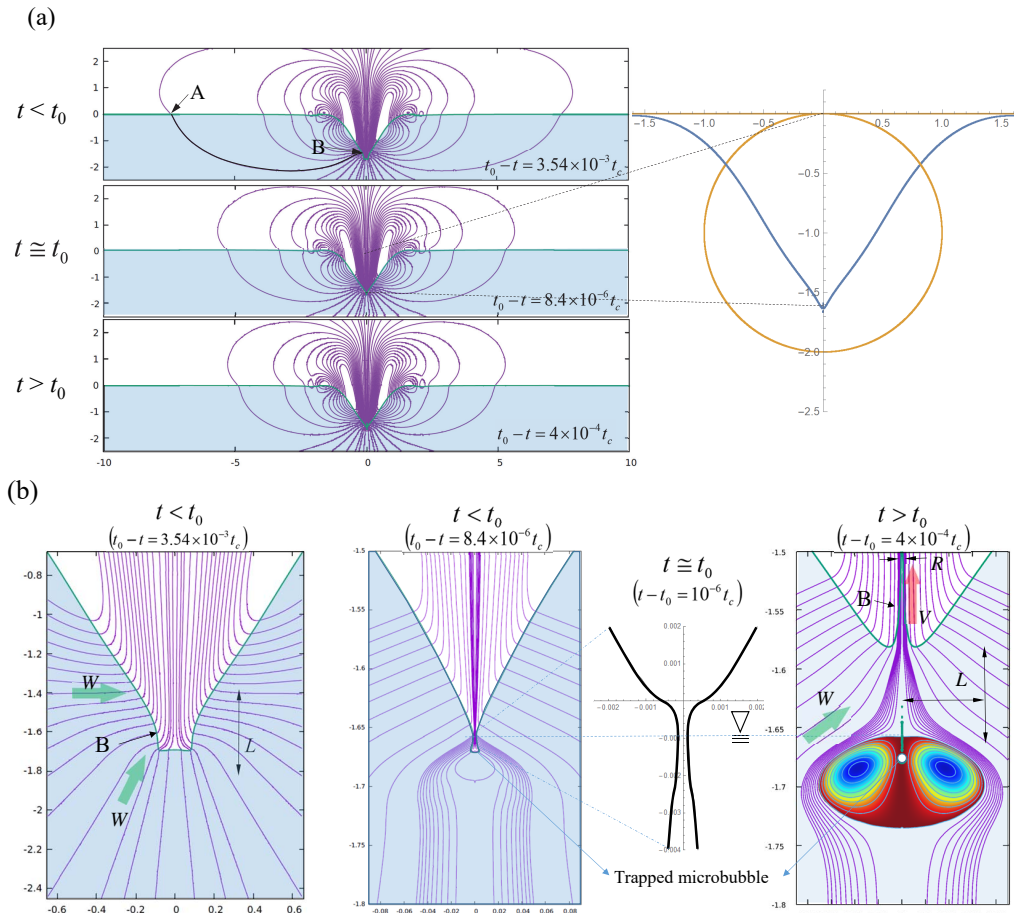


FIGURE 1. General overview of the flow development around the critical time t_0 of collapse of the main pilot wave at the bottom of the cavity, for $\text{Oh} = 0.032$, $\text{Bo} = 0$. The three instants here illustrated are $t_0 - t = 3.54 \times 10^{-3} t_c$, $t_0 - t = 8.4 \times 10^{-6} t_c$, and $t - t_0 = 4 \times 10^{-4} t_c$: (a) Global flow streamlines (similar to dipole contours at a liquid-gas surface) showing a particular one (line A-B) ending at the point (B) just above where the collapse eventually occurs. (b) Local details of the same instants. The stream function levels showed are closer around the tiny trapped bubble to exhibit the vortex ring. Noteworthy, the upper axial point of the ellipsoid defining the vortex ring coincides with the point where the surface collapsed at $t = t_0$ and remains at that position: observe the horizontal line connecting the three panels of figure (b). The main flow velocities W (radial) and V (axial, ejection) are indicated. In these simulations using VOF (Basilisk, Popinet (2015)), the density and viscosity of the liquid is 1000 and 100 times that of the gas, respectively, to reflect similar relations to the air-salt water ones.

central argument in Gañán-Calvo (2017). Thus, L obviously changes with time around the instant of collapse. To look for symmetries around t_0 , let us consider two situations, one for $t < t_0$ and the other for $t > t_0$ such that their characteristic length scales L are the same (see figure 1). Then, one may estimate the characteristic values of each term of equation (2.2) for both $t < t_0$ and $t > t_0$.

For $t < t_0$, both the left integral and the kinetic energy term at B in (2.2) should scale as ρW^2 . The surface tension term at B should be proportional to σ/L , and the gravity term to $\rho g R_o$. Finally, the curvature of streamlines suggests that the viscous stresses should scale as $\mu W/L$ (boundary layers cannot be thinner than L , as shown by Gañán-Calvo (2018)), as it does the integral in the right hand side of (2.2). Thus, the overall

scaling balance of (2.2) can be expressed as:

$$\rho (W^2 + \beta_1 g R_o) \sim \sigma L^{-1} + \alpha_1 \mu W L^{-1}, \quad (2.3)$$

where prefactors α_1 and β_1 should be universal constants if our approach is correct. Using the natural length and velocity, $l_\mu = \mu^2/(\rho\sigma)$ and $v_\mu = \sigma/\mu$ respectively, and defining $\zeta = L/l_\mu$ and $\omega = W/v_\mu$, this equation can be written as:

$$\omega^2 + \epsilon_1 \sim (1 + \alpha_1 \omega) \zeta^{-1}, \quad (2.4)$$

where, for simplification, $\epsilon_1 = \beta_1 \text{Oh}^2 \text{Bo} \ll 1$.

When $t > t_0$, the vigorous ejection in the axial direction generates the new characteristic velocity V and radial size R scales of the liquid jet. To appraise physical symmetry, the scale of the radial velocity W in the bulk and the (new) axial scale of the jet L should be taken the same as their namesakes for $t < t_0$ (see central panel in figure 1(b) for $\text{Oh} = 0.032$, $\text{Bo} = 0$). Even before collapse, the flow develops a stagnant region in the liquid (Gañán-Calvo 2017) just below the collapsing point. From this point, a vortex ring of characteristic (growing) size L and speed W like those beautifully described by Maxworthy (1972) (see figure 4 of his work) develops. By virtue of total energy preservation (and assuming that the trapped microbubble is much smaller than the vortex), its mechanical energy $\rho W^2 L^3$ should mirror that of the vigorous microjet, $\rho V^2 R^2 L$. This comprehensible mechanical symmetry principle, subsequently demonstrated by numerical simulation, debunks the kinematic proposal of Gordillo & Rodriguez-Rodriguez (2019) (dissecting absolute and relative speeds is not trivial in these flows, as Maxworthy (1972) shows): if one observes the streamlines below the jet, it is completely fed by an axial stream coming from the utmost depths and surrounds the vortex ring (see figure 1b, right panel). Those streamlines should ultimately originate very far from the bubble at the free surface. In summary, one can write:

$$\rho V^2 R^2 L \sim \rho W^2 L^3 \implies V R \sim W L \implies v \chi \sim \omega \zeta \quad (2.5)$$

where $\chi = R/l_\mu$ and $v = V/v_\mu$. As a secondary consequence, the nearly conical surface *independently* raises at characteristic speed W due to the incoming nearly conical flow.

One can now estimate the scaling of the different terms of (2.2) for a streamline ending at a point B at the surface of the jet (see figure 1a), and write the following balance:

$$\rho (V^2 + \beta_2 g R_o) \sim \alpha_2 \sigma R^{-1} + \mu W L^{-1}, \quad (2.6)$$

which using natural scales reads:

$$v^2 + \epsilon_2 \sim \alpha_2 \chi^{-1} + \omega \zeta^{-1}, \quad (2.7)$$

where $\epsilon_2 = \beta_2 \text{Oh}^2 \text{Bo} \ll 1$. If the variables $\{v, \omega, \chi, \zeta\}$ are universal functions of time, i.e. if (2.4), (2.5) and (2.7) hold for sufficiently ample periods around the critical time t_0 , these balances can be converted into equations by assuming that $\{v, \omega, \chi, \zeta\}$ are affected by the appropriate universal prefactors. Thus, taking for instance ζ as an independent variable, neglecting gravity ($\epsilon_{1,2} = 0$) and considering the physically meaningful root of system (2.4), (2.5) and (2.7) one gets:

$$\begin{aligned} \chi &= \eta_1 \zeta^{5/4} + \frac{\alpha_1 \alpha_2}{4} \zeta - \frac{\eta_2 \alpha_2}{2} \zeta^{3/2}, \\ v &= \eta_1 \zeta^{-3/4} - \frac{\alpha_1 \alpha_2}{2} \zeta^{-1} + \frac{(\eta_2 + (\alpha_1/2) \zeta^{-1/2}) \alpha_2}{2} \zeta^{-1/2}, \\ \omega &= \zeta^{-1/2} \left(\eta_2 + (\alpha_1/2) \zeta^{-1/2} \right), \end{aligned} \quad (2.8)$$

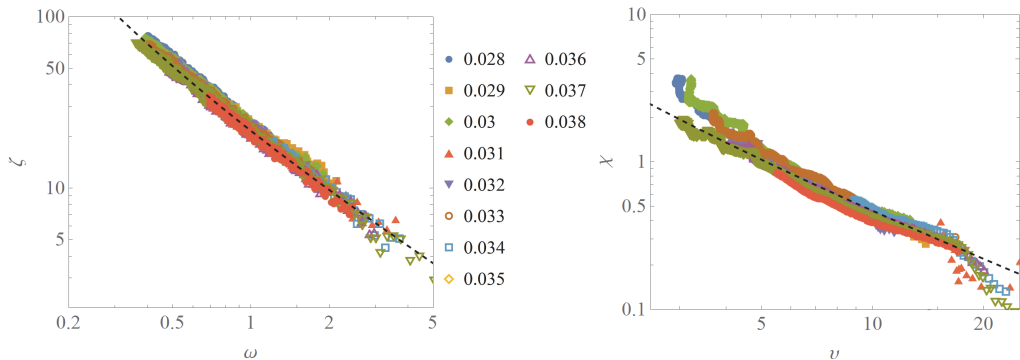


FIGURE 2. Numerical data (VOF, *Basilisk*, minimum cell size $3 \times 10^{-4} R_o$ for this figure) compared to prediction (2.8). (Left) ζ vs ω . (Right) χ vs v . The dashed lines are the theoretical predictions from the scaling analysis.

with $\eta_2 = \left(1 + \frac{\alpha_1^2}{4\zeta}\right)^{1/2}$ and $\eta_1 = \left(\left(\eta_2 + \frac{\alpha_1}{2\zeta^{1/2}}\right) + \alpha_2^2 \zeta^{1/2} \left(\eta_2 - \frac{\alpha_1}{2\zeta^{1/2}}\right)^2 / 4\right)^{1/2}$.

For $\alpha_{1,2} = 0$, (2.8) yields $\chi = v^{-5/3}$, $\zeta = v^{-4/3}$ and $\omega = v^{2/3}$, as predicted by Gañán-Calvo (2017): a test of consistency of that former study. To proof the accuracy of predictions (2.8), the time-dependent evolution of the scaling variables $\{\chi, \zeta, v, \omega\}$ is obtained from numerical simulation (VOF, *Basilisk*). To do so, we have recorded the time-dependent values of the radius of curvature and velocity of the jet front at the jet axis, and the meridional curvature at the point of maximum radial velocity of the free surface. They represent characteristic time-dependent values of R , V , L and W , respectively, for $t > t_0$ (no scales of R and V appear for $t < t_0$). Since (2.8) does not provide the time-dependencies of the variables, in figure 2 we plot the non-dimensional evolving values of ζ vs ω and χ vs v for a detailed range of Oh numbers around Oh_c . The best fitting prefactors of $\{\chi, \zeta, v, \omega\}$ are 0.055, 2.9, 15.0 and 1.2, respectively, assuming the values of $\alpha_{1,2}$ obtained from the experiments in the next section. Despite the deviations observed for the smallest and largest values of v , that reflect the vibrations of the droplet about pinch-off and ejection (not considered here) and the extremely rapid bubble pinching around $t = t_0$, respectively, the degree of collapse and fitting is remarkable.

2.1.1. Problem closure: ejected droplet size and speed

To close the problem, one can express the total energy equation in a sufficiently ample fluid volume $\Omega(t)$ around the initial bubble from the instant of bubble bursting ($t = 0$) up to an arbitrary t . To do so, the fluid volume $\Omega(t)$ can be a hemisphere around the cavity with a radius about twice or three times larger than R_o :

$$\int_{\Omega(t')} \rho \left(e + \mathbf{v}^2/2 + gz \right) d\Omega \Big|_{t=0}^t = - \int_{t=0}^t \int_{S(t')} \mathbf{v} \cdot (\boldsymbol{\tau}' - p\mathbf{I}) \cdot \mathbf{n} dA dt' \quad (2.9)$$

where $\boldsymbol{\tau}'$ is the viscous stress and \mathbf{I} the identity matrix. By the equilibrium of stresses at the free surface, the work made by the viscous forces is at most comparable to that made against the surface tension. Thus, the right hand side of 2.9 should always be proportional to a linear combination of σR_o^2 plus $\mu V_o R_o^2$, where V_o is an averaged characteristic speed in $\Omega(t)$. On the other hand, for $t < t_0$ (before the rapid ejection), the overall value of the left term would be proportional to $\rho V_o^2 R_o^3$. Given that the Ohnesorge numbers should necessarily be smaller than about 0.06 to have droplet ejection ($Oh = 0$ for the inviscid

case), and Bo numbers are always small for this problem as well, one would have:

$$\rho V_o^2 R_o^3 \sim \sigma R_o^2 \implies V_o \sim \left(\frac{\sigma}{\rho R_o} \right)^{1/2} \quad (2.10)$$

where V_o is, naturally, the capillary velocity. Thus, defining $V_o = \left(\frac{\sigma}{\rho R_o} \right)^{1/2}$, the viscous term will always be proportional to $\mu \left(\frac{\sigma R_o^3}{\rho} \right)^{1/2}$. In contrast, the volume integral in the left hand side of (2.9) should be proportional to $\rho V^2 R^2 R_o$ for $t > t_0$, since the ejection entails very large velocities V , despite $R \ll R_o$. If one neglects viscous and gravity works, (2.9) gives $\rho V^2 R^2 R_o \sim \sigma R_o^2$ which by virtue of (2.10) yields $VR \sim V_o R_o \sim (\sigma R_o / \rho)^{1/2} = \text{const.}$, consistently with the expected symmetry in this case. This relationship was already observed by Duchemin *et al.* (2002) and Ghabache *et al.* (2014), among others, for negligible viscosity and gravity. However, it does not faithfully describe the nonlinear behavior observed for non-zero Oh, especially around critical values of Oh (e.g. Duchemin *et al.* (2002); Walls *et al.* (2015); Ghabache & Séon (2016); Séon & Liger-Belair (2017); Gañán-Calvo (2017); Deike *et al.* (2018)). Thus, one should retain both Oh and Bo in (2.9). Hence, from (2.9) one finally has:

$$\rho (V^2 R^2 + \beta_3 g R_o^3) R_o \sim \alpha_3 \sigma R_o^2 - \mu V_o R_o^2 \quad (2.11)$$

where, again, prefactors α_3 and β_3 should be universal constants for very small gas-to-liquid density and viscosity ratios. The negative sign of the last term reflects that the extensional viscous stresses nearly everywhere at the inner surface of the fluid domain should point in the same direction as the velocity gradients (consistently with velocities increasing as $1/r^2$ for decreasing distances r), while the unit normal points in the opposite direction. (2.11) is equivalent to the energy equation in Gañán-Calvo (2017). Dividing by σR_o^2 , writing (2.11) in terms of the natural scales, and defining for convenience $\alpha_3 \equiv \text{Oh}^*$, one obtains

$$v^2 \chi^2 \sim \varphi - \beta_3 \text{Oh}^{-2} \text{Bo}, \quad (2.12)$$

where $\varphi = (\text{Oh}^* - \text{Oh})\text{Oh}^{-2}$. Interestingly, since both terms in (2.12) should be positive, it suggests the existence of a *maximum* value of the Ohnesorge, $\text{Oh}_{max} = \text{Oh}^* - \beta_3 \text{Bo}$, to have droplet ejection.

The system (2.4), (2.5), (2.7) and (2.12) has four roots, but just one physically meaningful. With the appropriate prefactors to have equalities and linearizing for Bo small, that root yields:

$$\begin{aligned} \chi &= k_r b \varphi \left((a^2 + \psi)^{1/2} + a \right)^{-1} (1 + \epsilon_r \text{Bo}), \\ v &= k_v b^{-1} \varphi^{-1/2} \left((a^2 + \psi)^{1/2} + a \right) / (1 + \epsilon_v \text{Bo}), \\ \zeta &= k_z b^{-2} \varphi^{3/4} \psi (1 + \epsilon_z \text{Bo}), \\ \omega &= k_w b^2 \varphi^{-1/4} \psi^{-1} (1 + \epsilon_w \text{Bo}), \end{aligned} \quad (2.13)$$

where $\psi = (b/\varphi^{1/4} - \varphi^{1/4}/b)^{-2}$, $b = \alpha_1^{1/2}$ and $a = b\alpha_2/2$. The six universal constants $\{\text{Oh}^*, \alpha_{i=1,2}, \beta_{i=1,2,3}\}$ will be obtained from experiments. The prefactors $k_{r,v,z,w}$ are time dependent such that the natural relationships (2.8) always hold, reaching to a fixed value just at the instant of droplet ejection. The algebraic relations among the fitting constants $\beta_{1,2,3}$ with $\epsilon_{r,v,z,w}$ are irrelevant here since the latter are the ones experimentally fitted. Moreover, when $\alpha_{i=1,2} \rightarrow 0$, one obtains $\chi = k_r \varphi^{5/4}$, $v = k_v \varphi^{-3/4}$, $\zeta = k_z \varphi$, and $\omega = k_w \varphi^{-1/2}$, exactly as proposed in Gañán-Calvo (2017). The overall consistency of

that initial proposal has already been verified by Lai *et al.* (2018), Deike *et al.* (2018), and Berny *et al.* (2020) among others; however, a full physical justification and further refinement was needed ahead of Gañán-Calvo (2017) and Gañán-Calvo (2018). As shown next, a fundamental aspect of the new solution (2.13) is its continuous validity for the complete Oh range, and appearance of a singularity when $\psi \rightarrow 0$, i.e. the existence of a critical Oh when $\varphi = b^4$, given by:

$$\text{Oh}_c = \left((1 + 4\alpha_1^2 \text{Oh}^*)^{1/2} - 1 \right) / (2\alpha_1^2) < \text{Oh}^*. \quad (2.14)$$

Close to this Oh_c , the local length scales of the flow become very small with a vanishing vortex ring and a very rapid, ballistic ejection of an extremely thin spout. This fundamental theoretical finding reveals a key physical symmetry reflected by the symmetry of ψ in (2.13), and justifies the experimental observations by many authors (Duchemin *et al.* (2002); Walls *et al.* (2015); Séon & Liger-Belair (2017); Ghabache & Séon (2016); Brasz *et al.* (2018); Deike *et al.* (2018); Berny *et al.* (2020), among others).

2.2. Experimental verification

To verify (2.13), six hundred experimental and numerical measurements of first ejected droplets and about one hundred of their corresponding initial velocities have been collected from the literature. The first ejected droplet radius R and its speed V data, expressed in non-dimensional form as $\chi/(1 + \epsilon_r \text{Bo})$ and $v(1 + \epsilon_v \text{Bo})$ at the time of ejection, respectively, are plotted in figure 3(a) and (b). To appraise the predicted theoretical singularity, extensive numerical solutions using VOF (*Basilisk*, momentum compensated) have been performed in the range $\text{Oh} \in (0.026, 0.05)$, for a gas-to liquid viscosity and density ratios equal to 0.01 and 0.001, respectively. We have increased the level of accuracy up to a minimum cell size $1.5 \times 10^{-4} R_o$ around the point of collapse and ejection (physically, around 2 nm for a gas bubble in water with $\text{Oh} = 0.033$). Our simulations clearly supports the existence of a singularity. The green lines are the theoretical predictions assuming constant liquid properties $\{\rho, \sigma, \mu\}$. The optimum fitting by least squares to our numerical simulations for $\text{Oh} \in (0.026, 0.05)$, and to the rest of data for $\text{Oh} < 0.028$ yields $\alpha_1 = 5$, $\alpha_2 = 0.25$ and $\text{Oh}^* = 0.062$. This gives $\text{Oh}_c = 0.0337$ for negligible gravity effects. The coefficients of the linear correction with Bo are $\epsilon_r = 0.4$, $\epsilon_v = 4$. As anticipated, the large data dispersion observed around the parametrical singularity (negligible Bo in all those cases) is consistent with the difficulty of measurements and simulations around the singularity, where the slightest effect (real or numerical) produces very large deviations. This includes the interaction with the gas environment, gas compressibility, and nonlinear effects (surfactants, viscosity, etc.). In addition, numerical simulations show the action of capillary waves faster than the average jet speed which reach the forming droplet: they may prevent or promote ejection when it is about to pinch-off. This provokes a noticeable oscillation of results around the theoretical prediction which should not affect its validity.

2.2.1. The critical Ohnesorge number. Resolving the paradox

A striking lack of agreement on the issue of the critical Oh has already been noticed in recent publications (Walls *et al.* 2015; Brasz *et al.* 2018; Deike *et al.* 2018; Gañán-Calvo 2017; Gañán-Calvo 2018; Gordillo & Rodríguez-Rodríguez 2019). Even the mere existence of any singularity has been questioned (Brasz *et al.* 2018; Gordillo & Rodríguez-Rodríguez 2019), arguing that a minimum finite value of the emitted droplet size should exist based on the role of viscous forces on the development of the liquid jet (Brasz *et al.* 2018). However, figure 4 of Brasz *et al.* (2018) is consistent with a theoretical

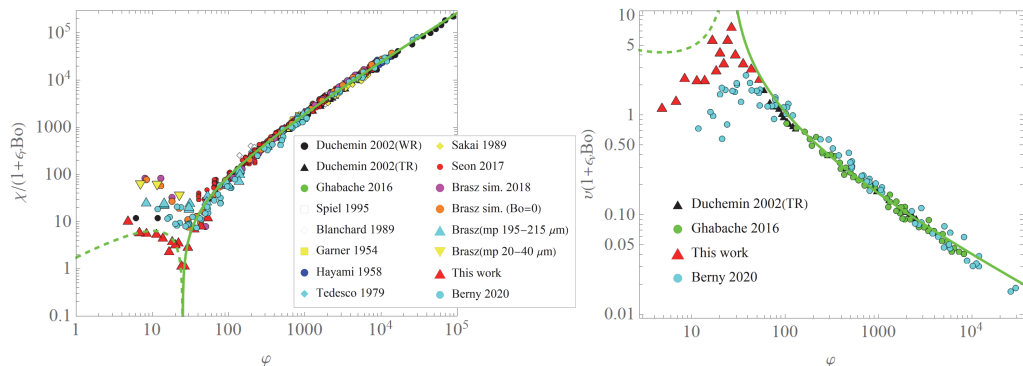


FIGURE 3. Experimental measurements from different literature sources (see Gañán-Calvo (2017) for additional information) of (Left) first ejected droplet size, and (Right) initial velocity of ejected droplets. The black line is the theoretical prediction in both plots.

vanishing of droplet sizes. Well before, figure 12 of Duchemin *et al.* (2002) clearly suggests the possibility of divergence of velocities, in the range of Oh between 0.03 and 0.04. Our scaling analysis, even in the linearized approximation assuming a small role of gravitational effects, resolves the paradox, explains the observed symmetry of behavior around Oh_c and provides a complete explanation for the appearance of a singularity. The possible effect of the outer gas environment on the critical Oh_c should also be considered. In addition, the complexity of the phenomenon is augmented including surface viscosity (Ponce-Torres *et al.* 2017), Marangoni and non-Newtonian effects (Sanjay *et al.* 2021), or the presence of immiscible liquids (Yang *et al.* 2020). These are subjects of subsequent studies.

This research has been supported by the Spanish Ministry of Economy, Industry and Competitiveness under Grants DPI2016-78887 and PID2019-108278RB, and by Junta de Andalucía under Grant P18-FR-3623.

REFERENCES

- BERNY, A., DEIKE, L., SÉON, T. & POPINET, S. 2020 Role of all jet drops in mass transfer from bursting bubbles. *Phys. Rev. Fluids* **5** (3).
- BLANCHARD, D. C. & WOODCOCK, A. H. 1957 Bubble formation and modification in the sea and its meteorological significance. *Tellus* **9** (2), 145–158.
- BOUROUBA, L. 2021 The fluid dynamics of disease transmission. *Annu. Rev. of Fluid Mech.* **53**, 473–508.
- BRASZ, C. F., BARTLETT, C.T., WALLS, P. L. L., FLYNN, E. G., YU, Y. E. & BIRD, J. C. 2018 Minimum size for the top jet drop from a bursting bubble. *Phys. Rev. Fluids* **3**.
- DASOUQI, A.A., YEOM, G.-S. & MURPHY, D.W. 2021 Bursting bubbles and the formation of gas jets and vortex rings. *Exp. Fluids* **62** (1).
- DEIKE, L., GHABACHE, E., LIGER-BELAIR, G., DAS, A. K., ZALESKI, S., POPINET, S. & SEON, T. 2018 Dynamics of jets produced by bursting bubbles. *Phys. Rev. Fluids* **3**.
- DUCHEMIN, L., POPINET, S., JOSSERAND, C. & ZALESKI, S. 2002 Jet formation in bubbles bursting at a free surface. *Phys. Fluids* **14** (9), 3000–3008.
- EGGERS, J. & FONTELOS, M. A. 2015 *Singularities: formation, structure and propagation*. Cambridge University Press.
- EGGERS, J., FONTELOS, M. A., LEPPINEN, D. & SNOEIJER, J. H. 2007 Theory of the collapsing axisymmetric cavity. *Phys. Rev. Lett.* **98**, 094502.
- FONTELOS, M. A., SNOEIJER, J. H. & EGGERS, J. 2011 The spacial structure of bubble pinch-off. *J. Appl. Math.* **71**, 1696–1716.

- GAÑÁN-CALVO, A. M. 2017 Revision of bubble bursting: universal scaling laws of top jet drop size and speed. *Phys. Rev. Lett.* **119**, 204502.
- GAÑÁN-CALVO, A. M. 2018 Scaling laws of top jet drop size and speed from bubble bursting including gravity and inviscid limit. *Phys. Rev. Fluids*. **3**, 091601.
- GAÑÁN-CALVO, A. M., REBOLLO-MUÑOZ, N. & MONTANERO, J. M. 2013 Physical symmetries and scaling laws for the minimum or natural rate of flow and droplet size ejected by Taylor cone-jets. *New J. Phys.* **15**, 033035.
- GHABACHE, E., ANTKOWIAK, A., JOSSEAND, C. & SÉON, T. 2014 On the physics of fizziness: How bubble bursting controls droplets ejection. *Phys. Fluids* **26**, 121701.
- GHABACHE, E., LIGER-BELAIR, G., ANTKOWIAK, A. & SÉON, T. 2016 Evaporation of droplets in a champagne wine aerosol. *Sci. Rep.* **6**, 25148.
- GHABACHE, E. & SÉON, T. 2016 Size of the top jet drop produced by bubble bursting. *Phys. Rev. Fluids* **1**, 051901.
- GORDILLO, J. M. & RODRIGUEZ-RODRIGUEZ, J. 2019 Capillary waves control the ejection of bubble bursting jets. *J. Fluid Mech.* **867**, 556–571.
- ISMAIL, A.S., GAÑÁN-CALVO, A.M., CASTREJÓN-PITA, J.R., HERRADA, M.A. & CASTREJÓN-PITA, A.A. 2018 Controlled cavity collapse: Scaling laws of drop formation. *Soft Matter* **14** (37), 7671–7679.
- KIENTZLER, C. F., ARONS, A. B., BLANCHARD, D. C. & WOODCOCK, A. H. 1954 Photographic investigation of the projection of droplets by bubbles bursting at a water surface. *Tellus* **6** (1), 1–7.
- LAI, CHING-YAO, EGGERS, JENS & DEIKE, LUC 2018 Bubble bursting: Universal cavity and jet profiles. *Phys. Rev. Lett.* **121**.
- LONGUET-HIGGINS, M. S. 1992 Capillary rollers and bores. *J. Fluid Mech.* **240**, 659–679.
- MAXWORTHY, T. 1972 The structure and stability of vortex rings. *J. Fluid Mech.* **51** (1), 15–32.
- PONCE-TORRES, A., MONTANERO, J.M., HERRADA, M.A., VEGA, E.J. & VEGA, J.M. 2017 Influence of the surface viscosity on the breakup of a surfactant-laden drop. *Phys. Rev. Lett.* **118** (2).
- POPINET, S. 2015 Basilisk flow solver and PDE library. <http://basilisk.fr/>, accessed: 2021/02/24.
- SAMPATH, K., AFSHAR-MOHAJER, N., CHANDRALA, L.D., HEO, W.-S., GILBERT, J., AUSTIN, D., KOEHLER, K. & KATZ, J. 2019 Aerosolization of crude oil-dispersant slicks due to bubble bursting. *J. Geophys. Res.-Atmos.* **124** (10), 5555–5578.
- SANJAY, V., D.LOHSE & JALAAL, M. 2021 Bursting bubble in a viscoplastic medium. *arXiv:2101.07744v1*.
- SÉON, T. & LIGER-BELAIR, G. 2017 Effervescence in champagne and sparkling wines: From bubble bursting to droplet evaporation. *Eur. Phys. J. Special Topics* **226**, 117–156.
- VERON, F. 2015 Ocean spray. *Annu. Rev. Fluid Mech.* **47**, 507–538.
- WALLS, P. L. L., HENAU, L. & BIRD, J. C. 2015 Jet drops from bursting bubbles: How gravity and viscosity couple to inhibit droplet production. *Phys. Rev. E* **92**, 021002(R).
- YANG, Z.Q., TIAN, Y.S. & THORODDSSEN, S.T. 2020 Multitude of dimple shapes can produce singular jets during the collapse of immiscible drop-impact craters. *J. Fluid Mech.* .
- YARIN, A.L. 2006 Drop impact dynamics: Splashing, spreading, receding, bouncing. . . *Annu. Rev. Fluid Mech.* **38**, 159–192.
- ZEFF, B. W., KLEBER, B., FINEBERG, J. & LATHROP, D. P. 2000 Singularity dynamics in curvature collapse and jet eruption on a fluid surface. *Nature* **403**, 401–404.